HHS Public Access

Author manuscript

Mol Cancer Ther. Author manuscript; available in PMC 2017 October 01.

Published in final edited form as:

Mol Cancer Ther. 2016 October ; 15(10): 2521–2529. doi:10.1158/1535-7163.MCT-16-0258.

Preclinical Modeling of KIF5B-RET Fusion Lung Adenocarcinoma

Qingling Huang[1], **Valentina E. Schneeberger**[1], **Noreen Luetteke**[2], **Chengliu Jin**[3], **Roha Afzal**[2], **Mikalai M. Budzevich**[2], **Rikesh J. Makanji**[4], **Gary V. Martinez**[2,5], **Tao Shen**[6], **Lichao Zhao**[7], **Kar-Ming Fung**[6,7], **Eric B. Haura**[8,9], **Domenico Coppola**[9,10], and **Jie Wu**[1,6,7,9,*]

[1]Department of Molecular Oncology, H. Lee Moffitt Cancer Center and Research Institute, Tampa, Florida

[2]Small Animal Modeling and Imaging Core, H. Lee Moffitt Cancer Center and Research Institute, Tampa, Florida

[3]Transgenic and Gene Targeting Core, Georgia State University, Atlanta, Georgia

[4]Department of Radiology, H. Lee Moffitt Cancer Center and Research Institute, Tampa, Florida

[5]Department of Cancer Imaging and Metabolism, H. Lee Moffitt Cancer Center and Research Institute, Tampa, Florida

[6]Peggy and Charles Stephenson Cancer Center, University of Oklahoma Health Sciences Center, Oklahoma City, Oklahoma

[7]Department of Pathology, University of Oklahoma Health Sciences Center, Oklahoma City, Oklahoma

[8]Department of Thoracic Oncology, H. Lee Moffitt Cancer Center and Research Institute, Tampa, Florida

[9]Department of Oncology Sciences, University of South Florida College of Medicine, Tampa, Florida

[10]Department of Anatomic Pathology, H. Lee Moffitt Cancer Center and Research Institute, Tampa, Florida

Abstract

RET fusions have been found in lung adenocarcinoma, of which KIF5B-RET is the most prevalent. We established inducible KIF5B-RET transgenic mice and KIF5B-RET-dependent cell lines for preclinical modeling of KIF5B-RET-associated lung adenocarcinoma. Dox-induced CCSP-rtTA/tetO-KIF5B-RET transgenic mice developed invasive lung adenocarcinoma with desmoplastic reaction. Tumors regressed upon suppression of KIF5B-RET expression. By culturing KIF5B-RET-dependent BaF3 (B/KR) cells with increasing concentrations of

[*]**Corresponding Author:** Jie Wu, Ph.D., Peggy and Charles Stephenson Cancer Center, University of Oklahoma Health Sciences Center, 975 N.E. 10th Street, BRC-411B, Oklahoma City, OK 73104, Telephone: (405) 271-8001, ext. 31092, Fax: (405) 271-2141, jie-wu@ouhsc.edu.

Disclosure of Potential Conflict of Interest

The authors declare no conflict of interest.

cabozantinib or vandetanib, we identified cabozantinib-resistant RET^{V804L} mutation and vandetanib-resistant-RET^{G810A} mutation. Among cabozantinib, lenvatinib, ponatinib, and vandetanib, ponatinib was identified as the most potent inhibitor against KIF5B-RET and its drug-resistant mutants. Interestingly, the vandetanib-resistant KIF5B-RET^{G810A} mutant displayed gain-of-sensitivity (GOS) to ponatinib and lenvatinib. Treatment of Dox-induced CCSP-rtTA/tetO-KIF5B-RET bitransgenic mice with ponatinib effectively induced tumor regression. These results indicate that KIF5B-RET-associated lung tumors are addicted to the fusion oncogene and ponatinib is the most effective inhibitor for targeting KIF5B-RET in lung adenocarcinoma. Moreover, this study finds a novel vandetanib-resistant RET^{G810A} mutation and identifies lenvatinib and ponatinib as the secondary drugs to overcome this vandetanib resistance mechanism.

Keywords

KIF5B-RET; fusion oncogene; lung adenocarcinoma; transgenic mice; protein tyrosine kinase inhibitor; drug resistance; mutation; ponatinib

Introduction

Lung adenocarcinoma is a major subtype of non-small cell lung cancer (NSCLC) with increasing incidence in many countries (1). Compared to other histological types of lung cancer, lung adenocarcinoma frequently harbors KRAS or protein tyrosine kinase (PTK) aberrations (2, 3). While mutant KRAS is difficult to target directly at present, PTKs are targetable, allowing precision treatment targeting individual patient's driver oncogene. Targeting PTK driver oncogenes with small molecule inhibitors in lung adenocarcinoma has shown clinical success in managing NSCLC. This is exemplified by EGFR and ALK inhibitor therapies in EGFR mutation and ALK-fusion lung adenocarcinoma (4, 5). However, acquired resistance to EGFR and ALK kinase inhibitors usually occur within a year after the drug treatment, making it necessary to use secondary drugs to prolong the therapeutic response (6, 7). Moreover, except for EGFR mutations and ALK fusions, other PTK alterations in lung adenocarcinoma occur at <3% rates (8, 9), rendering clinical studies of these PTK oncogenes difficult (10).

Several laboratories have identified recurrent RET fusion genes in 1–2% of lung adenocarcinoma cases (8, 11–14). Among the fusion partners, KIF5B is the most prevalent. RET rearrangements in lung adenocarcinoma are mutually exclusive from other known driver oncogenic mutations, including KRAS, EGFR, ALK, BRAF, and ERBB2 (8). Moreover, ALK, RET, and ROS1 oncofusion-associated lung adenocarcinoma tissues harbor significantly fewer mutations than other lung adenocarcinoma tissues (10). This suggests a strong role of these fusion oncogenes in driving the tumors, implicating them as excellent therapeutic targets.

A number of PTK inhibitors (TKIs) are known to cross-inhibit RET kinase activity (15). These include cabozantinib and vandetanib that have been approved by the United States Food and Drug Administration for the treatment of advanced medullary thyroid cancer, which carries RET point mutations in 30–50% of cases (15). So far, two reports have

described the responses of 6 RET-fusion lung adenocarcinoma patients treated with cabozantinib: 4 patients had partial responses and 2 patients had stable disease (16, 17). One patient with RET-fusion lung adenocarcinoma who received vandetanib was reported to have decreased tumor size (18). These are encouraging initial findings but more studies are needed. Several clinical trials of RET kinase inhibitors are ongoing (8, 15). However, the rarity of this molecular subtype of the disease presents a barrier for the current and future clinical studies, as it will take a long time to enroll adequate number of patients into the clinical trials.

To generate a preclinical model of RET fusion lung adenocarcinoma in an immune competent environment, we generated tetO-KIF5B-RET transgenic mice and used CCSP-rtTA/tetO-KIF5B-RET bitransgenic mice to induce KIF5B-RET expression in the lungs by doxycycline (Dox). We found that KIF5B-RET induced invasive lung adenocarcinoma with desmoplastic reaction. After tumor development, continuous expression of the KIF5B-RET fusion gene is required to maintain the lung tumors. Using a parallel *in vitro* cell-based assay, we identified ponatinib as the most potent inhibitor against KIF5B-RET, its kinase gatekeeper mutations, and a novel vandetanib-resistant RET^{G810A} mutant. Treatment of Dox-induced CCSP-rtTA/tetO-KIF5B-RET transgenic mice with ponatinib resulted in tumor regression.

Materials and Methods

Reagents

Antibodies to phospho-RET(Tyr905) and cleaved-PARP were from Cell Signaling Technology, antibodies to Flag-tag and β-actin were from Sigma, anti-RET antibody was from Santa Cruz Biotech. Anti-TTF1 (ab137061) antibody was from Abcam. Anti-cytokeratin antibody was from Dako (cat. No. Z0622). Ponatinib was from LC Laboratories. Cabozantinib, vandetanib, and lenvatinib were from Selleckchem.

Generation of transgenic mice

The KIF5B-RET (K15;R12, RET51 long form) (12) coding region with a Flag tag coding sequence at the C-terminus was synthesized by GeneArt Gene Synthesis (Life Technologies) and cloned into the L3/L2 loxP-tetO plasmid (19). The 6.6-kb BssHII tetO-KIF5B-RET transgene cassette (Fig. 1A) DNA fragment was used to generate tetO-KIF5B-RET transgenic mice in FVB/N strain as described in Supplementary Information.

Bitransgenic CCSP-rtTA/tetO-KIF5B-RET (C/KR) mice were produced by crossing tetO-KIF5B-RET mice with CCSP-rtTA mice (also in FVB/N strain) (19–21) (Fig. 1B). To induce KIF5B-RET expression, C/KR mice at 4 weeks old were fed with rodent chow containing 200 mg/kg Dox (Dox diet, Bio-Serv). Both male and female mice were used in the experiments.

Genotyping of CCSP-rtTA transgenic mice was as described previously (19, 21). Genotyping of tetO-KIF5B-RET transgenic mice was performed using GoTaq Hot Start Green Master Mix (Promega) using primer pairs: K5R-3T, 5’-CACGAGAGCTGATGGCACTAACACT and TETO-3B, 5’-

CACAGCCCAGCCCAGCCCTCTACT. The 25 μl PCR reaction protocol was: 3 min at 94 °C, 30 cycles of 94 °C for 30 sec, 57 °C for 30 sec and 72 °C for 30 sec with a final extension step of 72 °C for 5 min, which yielded a 309-bp product. Animal experiments were approved by the Institutional Animal Care and Use Committee of University of South Florida.

Cell cultures and analyses

The mouse BaF3 cells were obtained from Dr. H.G. Wang (H. Lee Moffitt Cancer) in 2000 and have been stored in liquid nitrogen. BaF3 cells were cultured in RPMI-1640/10% fetal bovine serum (FBS) supplemented with 2 ng/ml interleukin-3 (IL-3) as described (22). The identity of BaF3 cells were evaluated based on their dependency on mouse IL-3. The authors have not authenticated BaF3 cells using DNA-based method. To generate KIF5B-RET-transformed BaF3 cells (B/KR), BaF3 cells were infected with lentiviruses containing a flag-tagged KIF5B-RET gene. Individual puromycin-resistant cell lines were isolated, screened for the presence of KIF5B-RET by immunoblotting, and evaluated for IL-3-independence.

To identify drug-resistant mutations, established B/KR cells were incubated with increasing concentrations of cabozantinib or vandetanib in RPMI-1640/10%FBS as described in the Results. Individual drug-resistant cell lines were isolated from semi-solid methylcellulose cultures, which contained 4:6 ratio of MethoCult H4100 (Stemcell Technologies) and 20%FBS in RPMI-1640. Genomic DNA of drug-resistant cell lines was isolated and the RET kinase domain coding region was sequenced in both strands of DNA following PCR amplification as described (23).

To determine drug sensitivity, B/KR cells (1,500 cells/well) were incubated in RPMI-1640/10% FBS in the presence of indicated concentrations of drugs in 96-well plates in triplicates. On day 5, viable cells were measured using the CellTiter-Glo reagent (Promega). IC_{50} measurements were obtained from at least two independent experiments.

Analyses of cell lysates by immunoprecipitation and immunoblotting were as described (19, 21, 23). Immune complex kinase assay using GST-Gab1 as the substrate was performed as described previously (24).

Histological examination

Mice were euthanized by CO_2 asphyxiation. Lungs were flushed with 10 ml phosphate-buffered saline and insufflated with 10% buffered formalin. After fixing overnight in 10% buffered formalin, paraffin blocks were prepared. Tissue sections were stained with hematoxylin and eosin (H&E). H&E stain tissue slides were examined by three pathologists and scanned using a ScanScope XT (Aperio). The Genie V1 histology pattern recognition software (Aperio) was used to segment hyperproliferative lesions/tumors from other lung tissue areas and background using the same parameters as described previously (21). Trichrome staining was performed by the Tissue Pathology Core at Stephenson Cancer Center.

Immunohistochemistry (IHC) was performed with a Leica Bond III automated IHC protocol using a Leica Bond-III Polymer Refine Detection reagents (Cat. No.: DS 9800). Epitope

retrieval was citrate buffer (pH 6.0) at 100 °C for 20 min. Anti-TTF1 and anti-cytokeratin antibodies were used at 1:400 dilution for 30 min.

Magnetic resonance imaging (MRI) and computerized tomography (CT) protocols

For MRI, mice were anesthetized with 2% isoflurane and transferred to mouse cradle mounted on an insertion device and positioned within the RF coil of the magnet and kept under anesthesia for the duration of the experiment. The mice were physiologically monitored and maintained with a Model 1030 Monitoring and Gating System (SA Instruments, Inc). A respirator sensor pad was placed under each animal to manually control anesthesia mixture whereas a fiber optic rectal thermometer was used for temperature feedback control, which was set to maintain a body temperature of 37 ± 1 °C. Respiration rate was maintained at 50 – 60 breaths per minute and respiratory-gated MR images were acquired during the resting phase after exhalation. MRI was performed using a 7-T horizontal magnet (ASR 310, Agilent Technologies) equipped with nested 205/120/HDS gradient insert in a bore size of 310 mm. Two RF coils, a 35-mm Litzcage coil (Doty Scientific, Inc.) and a 24-mm Litzcage coil (Doty Scientific, Inc), were used depending on the sizes and weights of the mice. Temperature control of the imaging gradients was achieved by means of a water chiller (Neslab Waters) and maintained at 12 °C for all experiments.

Coronal multislice T_2-weighted fast spin-echo (FSEMS) respiratory-gated sequences were acquired with TE/TR = 30.05/1497.60 ms, data matrix = 256×128, 20 slices, field of view (FOV) = 90×40 mm^2, 16 averages and slice thickness of 1.20 mm over about 10–12 minutes. In T_2–weighted images, tumor volumes and dimensions were quantified using manually drawn regions of interest (ROI) within lung on a slice-by-slice basis, where pixels above a given threshold were counted as part of diffuse lesions. Analysis was done with MATLAB™ using a script that employed multi-thresholding segmentation method from the image processing toolbox of MATLAB™. Care was taken to exclude the heart, vessels, and mediastinum.

For μCT, mice were scanned on an Inveon μCT scanner (Inveon micro CT/PET/SPECT, Siemens, Knoxville, TN, USA) using a free-breathing protocol. Animals were anesthetized with a mixture of 2% isoflurane and oxygen. Breathing rate was controlled by a BioVet physiological monitoring system (m2m Imaging Corporation, USA) and kept at average 60 breaths per minute. The 440 projections were taken over 220 degree arc trough 12 minutes over a FOV of 2.7 × 1.5 cm. The X-ray tube scanning parameters were 80 kVp voltage, 480 μA current, 1000ms exposure, we also applied 1.5 mm Al filter.

The acquired data were reconstructed 3D volume with dimensions 1024×576×441 voxels with 27.2669 um effective isotropic voxel size. CCD detector binning was 2×2. Reconstructed data of absorption coefficients were converted to Hounsfield units (HU) in range of −1000 Hu to 1000 HU, where the value of −1000 HU corresponds to the air and 0 HU corresponds to the water (we used 50 ml water phantom for calibration). Image data were evaluated by board certified radiologist using preclinical Inveon Research Workstation 3D Visualization module (Siemens, Knoxville, TN). The lung μCT images were viewed in

coronal, sagittal, and axial planes as well as in 3D. The 3D model of lung's air pathways were rendered from original HU data after applying intensity threshold procedure.

Statistical analysis

Statistical analyses were performed using unpaired t test with Welch's correction, without assuming equal SDs. The statistical significance was set to 0.05.

Results

Inducible KIF5B-RET transgenic mice

We generated a tetO-KIF5B-RET transgenic mouse line (A1) as described in the supplementary information. These monotransgenic mice had no detectable phenotype and no KIF5B-RET transcript in the tissues that we have examined (Fig. 1C, top panel). CCSP-rtTA/tetO-KIF5B-RET bitransgenic mice (C/KR) were generated by crossing tetO-KIF5B-RET mice with CCSP-rtTA mice (19, 20) and evaluated for Dox-induced expression of KIF5B-RET. As illustrated in Fig. 1C (bottom panel), Dox specifically induced KIF5B-RET mRNA in the lungs but not in the heart, intestine, liver, kidney, or spleen of C/KR mice. Immunoprecipitation of lung tissue lysates with an anti-Flag antibody followed by immunoblotting detected KIF5B-RET protein and phosphorylated KIF5B-RET in the lungs of Dox-induced C/KR mice (Fig. 1D).

In another microinjection experiment performed later, we obtained two other tetO-KIF5B-RET transgenic mouse lines (A2, G6). CCSP-rtTA/tetO-KIF5B-RET bitransgenic mice generated from A2 and G6 lines displayed the same phenotype as that observed in the A1 line (Supplementary Fig. 1). Since the A1 line was generated much earlier, Most of our experiments were conducted using this line.

KIF5B-RET transgenic mice develop lung adenocarcinoma with desmoplastic reaction

As early as one month after Dox induction, the lungs of C/KR bitransgenic mice developed areas of hyperplastic and early tumor lesions that were often accompanied by thickening of pleural stroma (Fig. 2A). Pleural thickening was observed in human lung adenocarcinoma harboring RET fusion (Supplementary Fig. 2A). By 4–5 months after Dox induction of KIF5B-RET expression, extensive lung tumors were observed in these C/KR mice (Fig. 2B, C). These tumors displayed predominantly lepidic growth pattern with focal solid pattern, visceral pleural involvement, and desmoplastic reaction (Fig. 2B, C). Lymphocytes were often observed near the desmoplastic reaction areas and macrophages were observed in the tumor lesion areas. In total, we examined 12 lungs from C/KR mice induced with Dox for 4–7 months (4 four months, 6 five months, 1 six months, and 1 seven months). Invasive tumors were observed in all 12 lungs, which were confirmed by cytokeratin IHC in every case. We have not observed metastasis of tumors to distal organs. However, we have not ruled out the possibility that distal metastasis may occur when the Dox-induced C/KR mice are kept for a longer period of time.

Desmoplastic reaction is associated with invasive lung adenocarcinoma in human lung cancer patients (Supplementary Fig. 2B) and was reported in the first case of KIF5B-RET

lung adenocarcinoma when KIF5B-RET fusion was discovered (14). In the Cancer Genome Atlas (TCGA) Research Network lung adenocarcinoma study (2), desmoplastic stroma are visible in the tissue sections of RET-fusion lung adenocarcinoma cases (Supplementary Fig. 2A).

Desmoplastic reaction also occurred in the lung tumors in Dox-induced C/KR mice derived from Line A2 and Line G6 of tetO-KIF5B-RET transgenic mice (Supplementary Fig. 1A, B). In comparison, we have not observed desmoplastic reaction in lung adenomas and adenocarcinomas in $Kras^{LA1}$ mice that express $Kras^{G12D}$ (25) (~ 6 months of age, Supplementary Fig. 1C), Dox-induced CCSP-rtTA/tetO-$EGFR^{L858R}$ transgenic mice (21, 26), or Dox-induced CCSP-rtTA/tetO-$SHP2^{E76K}$ transgenic mice (19) (n >20 lungs examined in each case).

The KIF5B-RET oncogene is required to maintain lung tumors

To determine if lung tumors in Dox-induced C/KR mice were addicted to the KIF5B-RET oncogene, we identified 7 Dox-induced C/KR mice (4–5 months) with MRI-detectable lung tumors. These mice were then fed regular chow without Dox. One month after Dox withdrawal, these mice were examined by MRI again. Lung tissue sections were examined by histology and tissue lysates analyzed by immunoprecipitation and immunoblotting for the expression of RET.

As shown in Fig. 3A, Dox withdrawal resulted in regression of MRI-detected tumor lesions in all 7 mice. Lungs from 5 of these mice were examined by histology as illustrated in Fig. 3B. The remaining lesions in the lungs from Dox withdrawn mice were mostly of incompletely resolved fibrotic tissues. Using a histology pattern recognition program (Aperio) as described previously (21), the hyperproliferation/tumor lesion areas were semi-quantified. The area of interest (AOI), which included some of bronchiolar epithelia in addition to hyperproliferation/tumor lesions, in these 5 lungs was 4.33±1.76% (mean ± std). In comparison, the AOI from 5 Dox-induced C/KR mice was 38.80±25.34%, whereas the AOI from the 5 wildtype mice was 2.47%±1.17%. Thus, Dox withdrawal from C/KR mice resulted in a significant reduction ($p = 0.008$) in the AOI to a level similar to that of normal wildtype mice ($p = 0.98$) (Fig. 3B).

Both KIF5B-RET protein and phosphorylated (pY905) KIF5B-RET were detected in Dox-induced C/KR mice (Fig. 3C). They were no longer detected in the lungs one month post-Dox withdrawal. Taken together, these data show that after tumor formation, continuous expression of KIF5B-RET is required to maintain the lung tumors.

Ponatinib is the most potent KIF5B-RET kinase inhibitor

BaF3 cells depend on IL-3 for survival. We established stable BaF3 cells expressing KIF5B-RET (B/KR). When cells were incubated in medium without IL-3, the parental cells and vector-control cells underwent apoptosis in 6 hours as measured by PARP cleavage, whereas B/KR cells continued to grow (Fig. 4A, B). Thus, KIF5B-RET transformed BaF3 cells into cytokine-independence. The KIF5B-RET transformation was inhibited by cabozantinib that suppressed the KIF5B-RET kinase activity (Fig. 4C, D).

Cabozantinib and vandetanib inhibited B/KR cells with IC_{50s} of 0.175 μM and 0.90 μM, respectively. To isolate cabozantinib- or vandetanib-resistant KIF5B-RET mutations, we incubated B/KR cells (2×10^7 cells) with sequentially increasing concentrations of cabozantinib (from 0.175 μM to 0.65 or 0.85 μM in two independent experiments) or vandetanib (from 0.90 μM to 4.5 or 5.5 μM in two independent experiments). Individual drug resistant cells were cloned by methylcellulose culture. After verification of constitutive KIF5B-RET tyrosine kinase activity in these cells in the presence of cabozantinib or vandetanib in the culture medium (Supplementary Fig. 3A), the protein tyrosine kinase domain coding regions of KIF5B-RET from these drug-resistant cell clones were sequenced. The RET^{V804L} gatekeeper mutation was identified in all 10 cabozantinib-resistant cell lines. A novel RET^{G810A} mutation was found in 8 of 10 vandetanib-resistant cell lines. We next immunoprecipitated KIF5B-RET, KIF5B-RET^{V804L}, and KIF5B-RET^{G810A} from these cells and assayed their PTK activity *in vitro* in the presence of increasing concentrations of cabozantinib or vandetanib. The results confirmed that KIF5B-RET^{V804L} was resistant to cabozantinib and that KIF5B-RET^{G810A} was resistant to vandetanib (Supplementary Fig. 3B).

To confirm that the novel RET^{G810A} mutation renders vandetanib resistance and to evaluate if drug resistance may be attributed to overexpression of KIF5B-RET protein, we recreated a BaF3/KIF5B-RET^{G810A} cell line (B/$KR^{G810A\text{-}REC}$) using lentivirus encoding the KIF5B-RET^{G810A}. We then compared expression of KIF5B-RET and KIF5B-RET^{G810A} protein in these cells and vandetanib resistance between B/KR^{G810A} and B/$KR^{G810A\text{-}REC}$. As shown in Supplementary Fig. 3C, KIF5B-RET and KIF5B-RET^{G810A} protein levels were similar between B/KR and the B/KR-derived B/KR^{G810A} cells. The independently generated B/$KR^{G810A\text{-}REC}$ cells had a 20% higher level of KIF5B-RET^{G180A} protein. The vandetanib IC_{50s} were 5.310 μM and 5.675 μM for B/KR^{G810A} and B/$KR^{G810A\text{-}REC}$ cells (sFig. 3D). These data confirm that the RET^{G810A} mutant is resistant to vandetanib. While we do not rule out the possibility that increased KIF5B-RET expression may confer some extent of drug tolerance, our results indicate that vandetanib resistance of B/KR^{G810A} cells is mainly due to the G810A mutation.

Cabozantinib, vandetanib, ponatinib and lenvatinib are multi-kinase TKIs that have been reported in on-going clinical trials of RET-fusion NSCLC (15). We compared these four drugs in the KIF5B-RET-dependent growth of B/KR cells. As shown in Fig. 4D, ponatinib was the most potent inhibitor with an IC_{50} of 0.07 μM for B/KR cells. B/KR^{V804L} gatekeeper mutation cells were pan-resistant to all four TKIs, resulting in 6.2, 8.7, 15.7, and 76-fold increase in IC_{50s} for ponatinib, vandetanib, cabozantinib, and lenvatinib, respectively (Fig. 4D). However, ponatinib had the least fold increase in IC_{50} and remained the most potent inhibitor for B/KR^{V804L} cells with a sub-micromolar IC_{50}.

Vandetanib IC_{50} for B/KR^{G810A} cells was increased 5.7-fold to 5.1 μM compared to B/KR cells. Interestingly, while cabozantinib had similar IC_{50s} in B/KR^{G810A} cells and B/KR cells, ponatinib and lenvatinib had lower IC_{50s} in B/KR^{G810A} cells by 8.7- and 3.6-folds, respectively. Thus, while the RET^{G810A} mutation causes vandetanib resistance, it becomes hypersensitive to ponatinib and lenvatinib. We hereby term this type of mutation as a gain-of-sensitivity (GOS) mutation.

To further compare the potencies of these four drugs for RET and RET^{V804L} and also to determine the potencies of these drugs for another known RET gatekeeper mutant RET^{V804M}, IC_{50s} for inhibition of recombinant RET, RET^{V804L}, and RET^{V804M} in an *in vitro* kinase assay were measured in parallel via a commercial service (Reaction Biology, Malvern, PA). As shown in Supplementary Fig. 4, ponatinib again displayed the most potent inhibitory activities against RET, RET^{V804L}, and RET^{V804M} among these four compounds.

Ponatinib induces lung tumor regression in Dox-induced C/KR bitransgenic mice

Since ponatinib was the most potent TKI for KIF5B-RET and its gatekeeper mutations, we chose it for the *in vivo* study in our KIF5B-RET transgenic animal model of NSCLC. Dox-induced C/KR mice (4–5 months) were examined by MRI and micro-CT. Eight mice with MRI-detected lung tumor lesions were divided into two groups and treated with ponatinib or vehicle (4 mice/group) by oral gavage (30 mg/kg/day, 5 days/week) (see Supplementary Fig. 5 for treatment schedule and body weight monitoring data). After 4 weeks of drug treatment, the lungs of these mice were examined again by MRI and μCT, and lung tissue sections were analyzed by histology.

Lung tumor lesions in the vehicle-treated mice were similar or worse based on MRI and μCT examination (Fig 5A, B, Supplementary Fig. 6, 7, Supplementary Information 2, sMovie). In contrast, the lung lesions were greatly reduced in ponatinib-treated mice. Semi-quantitative measurement of tumor lesions by MRI showed that the mean VOI was significantly ($p = 0.0286$) decreased from 494±83 mm^3 (prior to treatment) to 68±51 mm^3 (post treatment) in the ponatinib-treated cohort (Fig. 5B). In comparison, the mean MRI VOI was not significantly changed ($p = 0.6571$) in the vehicle-control cohort before (580±227 mm^3) and after (480±176 mm^3) treatment. Analysis of H&E stained lung tissue sections (Supplementary Fig. 6) by the histology pattern recognition program show that vehicle-treated cohort had a mean 23.25±3.20% of AOI with hyperplasia or neoplasia, whereas ponatinib-treated mice had significantly ($p = 0.0286$) less AOI (mean = 2.79±0.63%) similar to that of the wildtype mice (2.47%±1.17%, Fig. 3B, 5C). In another experiment, lung tissue lysates from Dox-induced C/KR mice treated with vehicle or ponatinib for 1 month were analyzed for tyrosine phosphorylation of KIF5B-RET. As shown in Fig. 5D, KIF5B-RET protein was decreased and its tyrosine phosphorylation was suppressed in the lungs of ponatinib-treated animals. Thus, ponatinib is effective in inhibiting KIF5B-RET kinase activity and reducing the lung tumors of C/KR mice.

Discussion

RET oncogene fusions occur in 1–2% of lung adenocarcinoma. The rarity of the molecular lesion presents a barrier for clinical studies of RET fusion-associated lung adenocarcinoma (10). To facilitate *in vivo* studies of RET-associated lung adenocarcinoma, we have established an inducible transgenic mouse model of KIF5B-RET-associated lung adenocarcinoma.

KIF5B-RET displayed a constitutively active PTK activity as measured by pRET when it was expressed in the lungs of Dox-induced C/KR transgenic mice. Hyper-proliferative lesions and early tumors in the lungs were observed as early as one month after Dox

induction of the C/KR mice, and progressed to invasive lung tumors in 4–5 months after Dox induction of KIF5B-RET expression in the C/KR mice. Lung tumors formed in this Dox-induced C/KR model resemble human invasive lung adenocarcinoma and are associated with desmoplastic reaction and visceral pleural involvement. Desmoplastic stroma was also evident in the RET fusion-positive lung adenocarcinoma cases in TCGA. Various histological patterns of RET fusion-positive lung adenocarcinoma have been observed, including the prevalence of poorly differentiated, solid-predominant histologic features in RET fusion cases of lung adenocarcinoma (17, 27–29). Lung tumors in our C/KR mouse model recapitulate the invasive desmoplastic feature of RET fusion-associated tumors.

Similar to the absence of desmoplastic stroma in the lung tumors of $Kras^{LA1}$ mice that we observed in this study, a previous study using the adenovirus-Cre recombinase/LSL-Ras^{G12D} mouse model also found that lung adenoma and adenocarcinoma developed in that mouse model lack stromal reaction (30). Knockout of tgfbr2 in the LSL-$Kras^{G12D}$ model allows the $Kras^{G12D}$-driven lung tumors to progress to invasive lung adenocarcinoma with desmoplastic reaction (30). Human NSCLC often can cause desmoplasia when they invade into stroma. Among 230 cases of human lung adenocarcinoma characterized in TCGA (2), there are 1 case with TGFBR2 deletion and 1 case with TGFBR2 point mutation (E257D), both of them occur in $KRAS^{G12C}$ tumors (www.cbioportal.org). While many other lung adenocarcinoma cases in the TCGA cohort show the desmoplastic histology, such as RET-fusion cases, they are not associated with TGFBR2 deficiency. Thus, although TGFBR2 deficiency could promote desmoplastic stroma deposition, other factors are also likely to contribute to the stromal response to the invasive tumors.

Genomic analysis has suggested the exclusive dependency of lung adenocarcinoma on ALK, RET, or ROS fusion oncogenes (10). Consistently, data from our Dox withdrawal experiment indicate that lung tumors developed in Dox-induced C/KR mice require the continuing expression of the KIF5B-RET fusion oncogene to maintain the malignancy. This property suggests that KIF5B-RET is an effective target for drug treatment to eliminate KIF5B-RET-associated lung adenocarcinoma.

By culturing KIF5B-RET-dependent B/KR cells with RET kinase inhibitors, we identified cabozantinib-resistant RET^{V804L} gatekeeper mutation and a novel vandetanib-resistant RET^{G810A} mutation. Interestingly, while the RET^{G810A} mutant remained sensitive to cabozantinib, it acquired GOS to ponatinib and lenvatinib. Recent clinical experience in EGFR and ALK inhibitor therapy of lung adenocarcinoma has shown that a major mechanism of developing drug resistance is secondary mutations in the targeted PTK kinase domain. Mutation-sensitive secondary TKIs can be developed and used to prolong the therapeutic response (31–33). Our finding here suggests that ponatinib or lenvatinib are the secondary drugs to use when RET^{G810A} mutation occurs in vandetanib-treated RET-associated cancer, including lung adenocarcinoma and metastatic thyroid cancer.

Among cabozantinib, lenvatinib, ponatinib, and vandetanib, our data show that ponatinib is the most potent inhibitor of RET PTK. Treatment of lung tumors induced by KIF5B-RET in the transgenic animals resulted in tumor regression. Thus, ponatinib is an effective drug for

treating KIF5B-RET-associated lung adenocarcinoma in this genetically engineered mouse model and is predicted to show anti-tumor efficacy in RET fusion lung adenocarcinoma patients. While the gatekeeper RET^{V804L} and RET^{V804M} mutations are less sensitive to ponatinib than the wildtype RET, ponatinib remains the most potent inhibitor (Fig. 4 and Supplementary Fig. 4). Thus, ponatinib appears to be the drug of choice for treating RET fusion-associated lung adenocarcinoma.

It is envisioned that more drugs will be developed, re-purposed, and evaluated for therapy of RET fusion-associated lung adenocarcinoma, either as novel single agent or in combination treatment. The immune competent C/KR mouse model that we developed here provides a resource allowing the direct side-by-side comparison of two drugs in preclinical studies or co-clinical trials (34, 35) of RET fusion-associated lung adenocarcinoma.

Supplementary Material

Refer to Web version on PubMed Central for supplementary material.

Acknowledgments

Financial information

This study was supported by National Institutes of Health grants R21CA175603 (to J. Wu), R01CA178456 (to J. Wu), P30CA076292 (to T. Sellers), P50CA119997 (to E. B. Haura), and P20GM103639 (to K.M. Fung).

We thank H. Lee Moffitt Cancer Center Core facility staff, including Animal, DNA sequencing, Histology, Microscopy Core facilities, and Stephenson Cancer Center/University of Oklahoma Health Sciences Center Histology Core facility staff for assistance. We also thank J.A. Whitsett for the CCSP-rtTA transgenic mice, D.C. Radisky and A.P. Fields for advice and assistance, and K. Politi and G. Felsenfeld for reagents.

Abbreviations list

AOI	area of interest
B/KR	BaF3/KIF5B-RET
CCSP	Clara cell secretory protein
C/KR	CCSP-rtTA/tetO-KIF5B-RET
CT	computerized tomography
Dox	doxycycline
GOS	gain-of-sensitivity
IHC	immunohistochemistry
IL-3	interleukin-3
MRI	magnetic resonance imaging
NSCLC	non-small cell lung cancer
PTK	protein tyrosine kinase

TCGA	the Cancer Genome Atlas
TKI	protein tyrosine kinase inhibitor

References

1. Nakamura H, Saji H. Worldwide trend of increasing primary adenocarcinoma of the lung. Surgery today. 2014; 44:1004–1012. [PubMed: 23754705]
2. Cancer Genome Atlas Research N. Comprehensive molecular profiling of lung adenocarcinoma. Nature. 2014; 511:543–550. [PubMed: 25079552]
3. Chen Z, Fillmore CM, Hammerman PS, Kim CF, Wong KK. Non-small-cell lung cancers: a heterogeneous set of diseases. Nat Rev Cancer. 2014; 14:535–546. [PubMed: 25056707]
4. Pao W, Chmielecki J. Rational, biologically based treatment of EGFR-mutant non-small-cell lung cancer. Nat Rev Cancer. 2010; 10:760–774. [PubMed: 20966921]
5. Friboulet L, Li N, Katayama R, Lee CC, Gainor JF, Crystal AS, et al. The ALK inhibitor ceritinib overcomes crizotinib resistance in non-small cell lung cancer. Cancer Disc. 2014; 4:662–673.
6. Riely GJ, Yu HA. EGFR: The Paradigm of an Oncogene-Driven Lung Cancer. Cli Cancer Res. 2015; 21:2221–2226.
7. Katayama R, Lovly CM, Shaw AT. Therapeutic targeting of anaplastic lymphoma kinase in lung cancer: a paradigm for precision cancer medicine. Cli Cancer Res. 2015; 21:2227–2235.
8. Kohno T, Nakaoku T, Tsuta K, Tsuchihara K, Matsumoto S, Yoh K, et al. Beyond ALK-RET, ROS1 and other oncogene fusions in lung cancer. Transl Lung Cancer Res. 2015; 4:156–164. [PubMed: 25870798]
9. Gainor JF, Shaw AT. Novel targets in non-small cell lung cancer: ROS1 and RET fusions. The Oncologist. 2013; 18:865–875. [PubMed: 23814043]
10. Saito M, Shimada Y, Shiraishi K, Sakamoto H, Tsuta K, Totsuka H, et al. Development of lung adenocarcinomas with exclusive dependence on oncogene fusions. Cancer Res. 2015; 75:2264–2271. [PubMed: 25855381]
11. Kohno T, Ichikawa H, Totoki Y, Yasuda K, Hiramoto M, Nammo T, et al. KIF5B-RET fusions in lung adenocarcinoma. Nat Med. 2012; 18:375–377. [PubMed: 22327624]
12. Takeuchi K, Soda M, Togashi Y, Suzuki R, Sakata S, Hatano S, et al. RET, ROS1 and ALK fusions in lung cancer. Nat Med. 2012; 18:378–381. [PubMed: 22327623]
13. Lipson D, Capelletti M, Yelensky R, Otto G, Parker A, Jarosz M, et al. Identification of new ALK and RET gene fusions from colorectal and lung cancer biopsies. Nat Med. 2012; 18:382–384. [PubMed: 22327622]
14. Ju YS, Lee WC, Shin JY, Lee S, Bleazard T, Won JK, et al. A transforming KIF5B and RET gene fusion in lung adenocarcinoma revealed from whole-genome and transcriptome sequencing. Genome Res. 2012; 22:436–445. [PubMed: 22194472]
15. Kohno T, Tsuta K, Tsuchihara K, Nakaoku T, Yoh K, Goto K. RET fusion gene: Translation to personalized lung cancer therapy. Cancer Sci. 2013; 104:1396–1400. [PubMed: 23991695]
16. Drilon A, Wang L, Hasanovic A, Suehara Y, Lipson D, Stephens P, et al. Response to Cabozantinib in patients with RET fusion-positive lung adenocarcinomas. Cancer Disc. 2013; 3:630–635.
17. Mukhopadhyay S, Pennell NA, Ali SM, Ross JS, Ma PC, Velcheti V. RET-rearranged lung adenocarcinomas with lymphangitic spread, psammoma bodies, and clinical responses to cabozantinib. J Thoracic Oncology. 2014; 9:1714–1719.
18. Gautschi O, Zander T, Keller FA, Strobel K, Hirschmann A, Aebi S, et al. A patient with lung adenocarcinoma and RET fusion treated with vandetanib. J Thoracic Oncology. 2013; 8:e43–e44.
19. Schneeberger VE, Luetteke N, Ren Y, Berns H, Chen L, Foroutan P, et al. SHP2E76K mutant promotes lung tumorigenesis in transgenic mice. Carcinogenesis. 2014; 35:1717–1725. [PubMed: 24480804]
20. Tichelaar JW, Lu W, Whitsett JA. Conditional expression of fibroblast growth factor-7 in the developing and mature lung. J Biol Chem. 2000; 275:11858–11864. [PubMed: 10766812]

21. Schneeberger VE, Ren Y, Luetteke N, Huang Q, Chen L, Lawrence HR, et al. Inhibition of Shp2 suppresses mutant EGFR-induced lung tumors in transgenic mouse model of lung adenocarcinoma. Oncotarget. 2015; 6:6191–6202. [PubMed: 25730908]
22. Dorsey JF, Cunnick JM, Lanehart R, Huang M, Kraker AJ, Bhalla KN, et al. Interleukin-3 protects Bcr-Abl-transformed hematopoietic progenitor cells from apoptosis induced by Bcr-Abl tyrosine kinase inhibitors. Leukemia. 2002; 16:1589–1595. [PubMed: 12200668]
23. Ren Y, Zhang Y, Liu RZ, Fenstermacher DA, Wright KL, Teer JK, et al. JAK1 truncating mutations in gynecologic cancer define new role of cancer-associated protein tyrosine kinase aberrations. Sci Rep. 2013; 3:3042. [PubMed: 24154688]
24. Ren Y, Meng S, Mei L, Zhao ZJ, Jove R, Wu J. Roles of Gab1 and SHP2 in paxillin tyrosine dephosphorylation and Src activation in response to epidermal growth factor. J Biol Chem. 2004; 279:8497–8505. [PubMed: 14665621]
25. Johnson L, Mercer K, Greenbaum D, Bronson RT, Crowley D, Tuveson DA, et al. Somatic activation of the K-ras oncogene causes early onset lung cancer in mice. Nature. 2001; 410:1111–1116. [PubMed: 11323676]
26. Politi K, Zakowski MF, Fan PD, Schonfeld EA, Pao W, Varmus HE. Lung adenocarcinomas induced in mice by mutant EGF receptors found in human lung cancers respond to a tyrosine kinase inhibitor or to down-regulation of the receptors. Genes Dev. 2006; 20:1496–1510. [PubMed: 16705038]
27. Tsai TH, Wu SG, Hsieh MS, Yu CJ, Yang JC, Shih JY. Clinical and prognostic implications of RET rearrangements in metastatic lung adenocarcinoma patients with malignant pleural effusion. Lung Cancer. 2015; 88:208–214. [PubMed: 25773866]
28. Tsuta K, Kohno T, Yoshida A, Shimada Y, Asamura H, Furuta K, et al. RET-rearranged non-small-cell lung carcinoma: a clinicopathological and molecular analysis. British J Cancer. 2014; 110:1571–1578.
29. Pan Y, Zhang Y, Li Y, Hu H, Wang L, Li H, et al. ALK, ROS1 and RET fusions in 1139 lung adenocarcinomas: a comprehensive study of common and fusion pattern-specific clinicopathologic, histologic and cytologic features. Lung Cancer. 2014; 84:121–126. [PubMed: 24629636]
30. Borczuk AC, Sole M, Lu P, Chen J, Wilgus ML, Friedman RA, et al. Progression of human bronchioloalveolar carcinoma to invasive adenocarcinoma is modeled in a transgenic mouse model of K-ras-induced lung cancer by loss of the TGF-beta type II receptor. Cancer Res. 2011; 71:6665–6675. [PubMed: 21911454]
31. Cross DA, Ashton SE, Ghiorghiu S, Eberlein C, Nebhan CA, Spitzler PJ, et al. AZD9291, an irreversible EGFR TKI, overcomes T790M-mediated resistance to EGFR inhibitors in lung cancer. Cancer Disc. 2014; 4:1046–1061.
32. Janne PA, Yang JC, Kim DW, Planchard D, Ohe Y, Ramalingam SS, et al. AZD9291 in EGFR inhibitor-resistant non-small-cell lung cancer. New England J Med. 2015; 372:1689–1699. [PubMed: 25923549]
33. Katayama R, Friboulet L, Koike S, Lockerman EL, Khan TM, Gainor JF, et al. Two novel ALK mutations mediate acquired resistance to the next-generation ALK inhibitor alectinib. Clin Cancer Res. 2014; 20:5686–5696. [PubMed: 25228534]
34. Chen Z, Cheng K, Walton Z, Wang Y, Ebi H, Shimamura T, et al. A murine lung cancer co-clinical trial identifies genetic modifiers of therapeutic response. Nature. 2012; 483:613–617. [PubMed: 22425996]
35. Chen Z, Akbay E, Mikse O, Tupper T, Cheng K, Wang Y, et al. Co-clinical trials demonstrate superiority of crizotinib to chemotherapy in ALK-rearranged non-small cell lung cancer and predict strategies to overcome resistance. Clin Cancer Res. 2014; 20:1204–1211. [PubMed: 24327273]

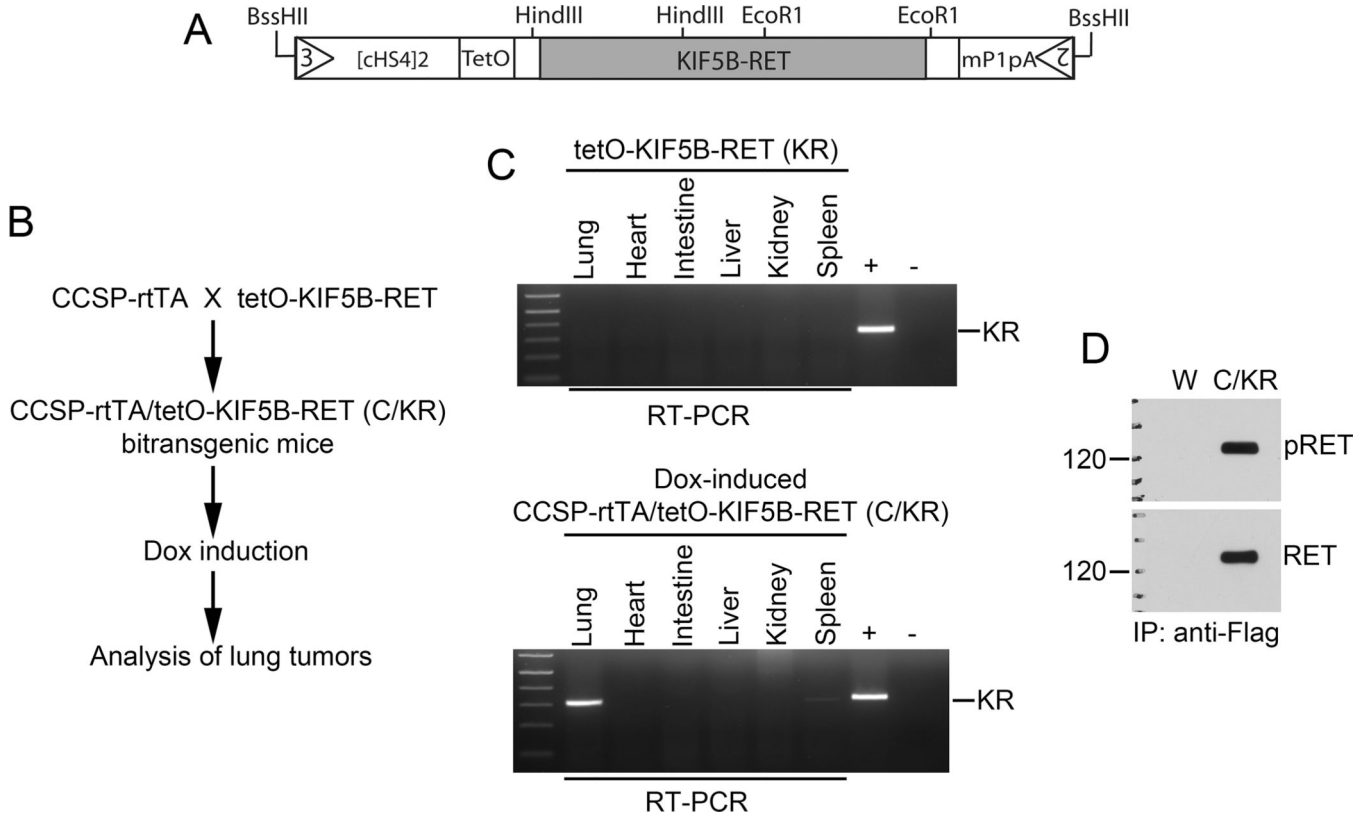

Figure 1.

Derivation and analysis of tetO-KIF5B-RET transgenic mice. A, schematic representation of tetO-KIF5B-RET transgene. B, scheme for production of C/KR bitransgenic mice and induction of the KIF5B-RET transgene expression in the mouse lung type II epithelial cells. C, RT-PCR analysis of KIF5B-RET mRNA expression in various tissues in monotransgenic tetO-KIF5B-RET mouse and in C/KR bitransgenic mouse fed with Dox diet for 1 month. D, after induction with Dox diet for 1 month, cell lysates were prepared from lung tissues of CCSP-rtTA/tetO-KIF5B-RET (C/KR) bitransgenic or wildtype (W) mice. Immunoprecipitation-immunoblotting analysis of KR expression and phosphorylation was performed.

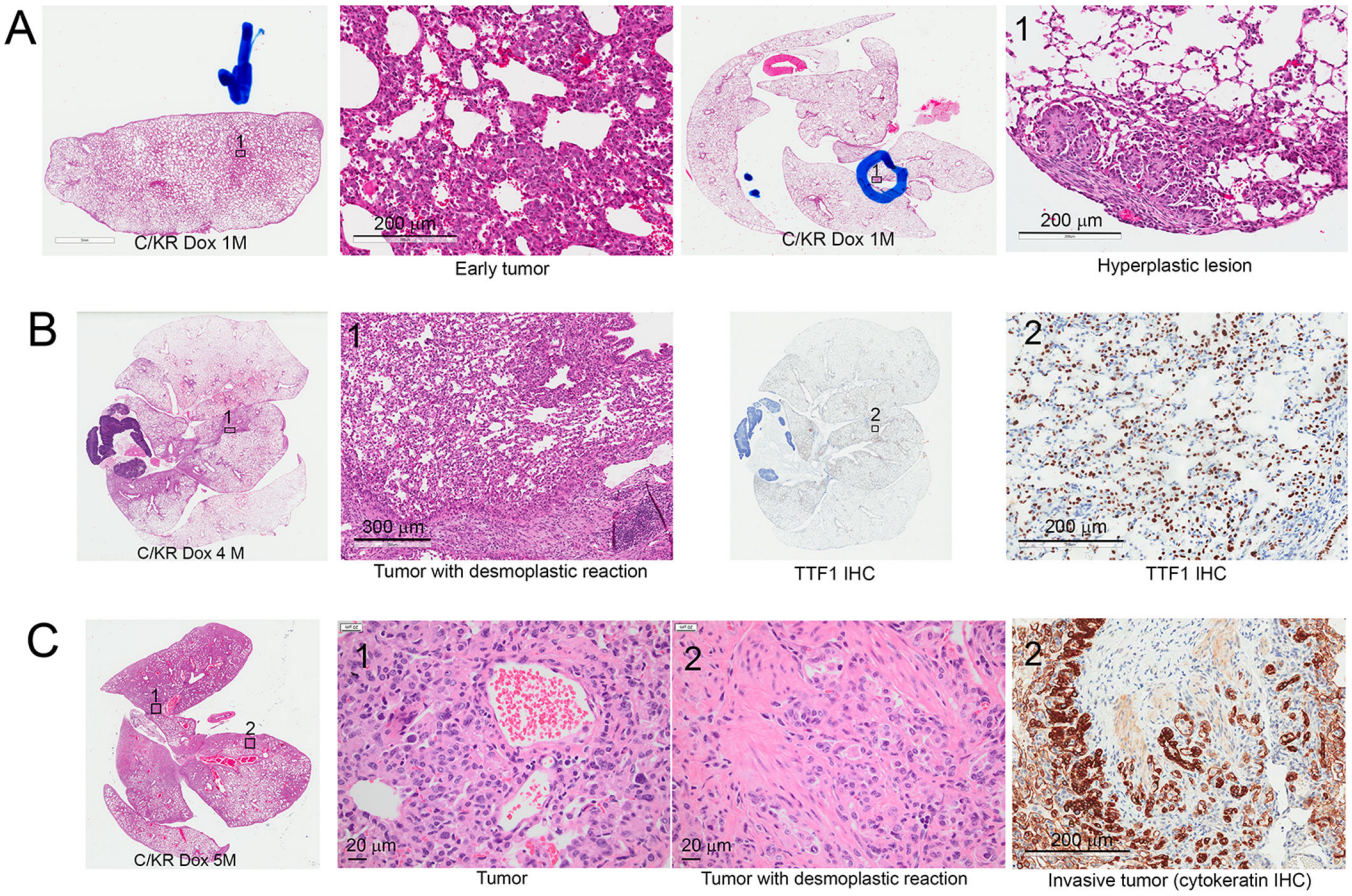

Figure 2.

Dox-induced bitransgenic C/KR mice develop lung tumors. A, H&E stained sections showing C/KR bitransgenic mice developed areas of hyperplastic lesions and early tumors after one month Dox induction. B, lung sections of a C/KR mouse induced with Dox for 4 months. Left, an H&E stained lung section showing lung with desmoplastic tumors. Right, tumor cells were stained positive of nuclear TTF1. C, lung sections of a C/KR mouse induced with Dox for 5 months. Right, H&E stained lung section with extensive tumors and desmoplasia. Right, cytokeratin stain confirmed invasive lung tumor.

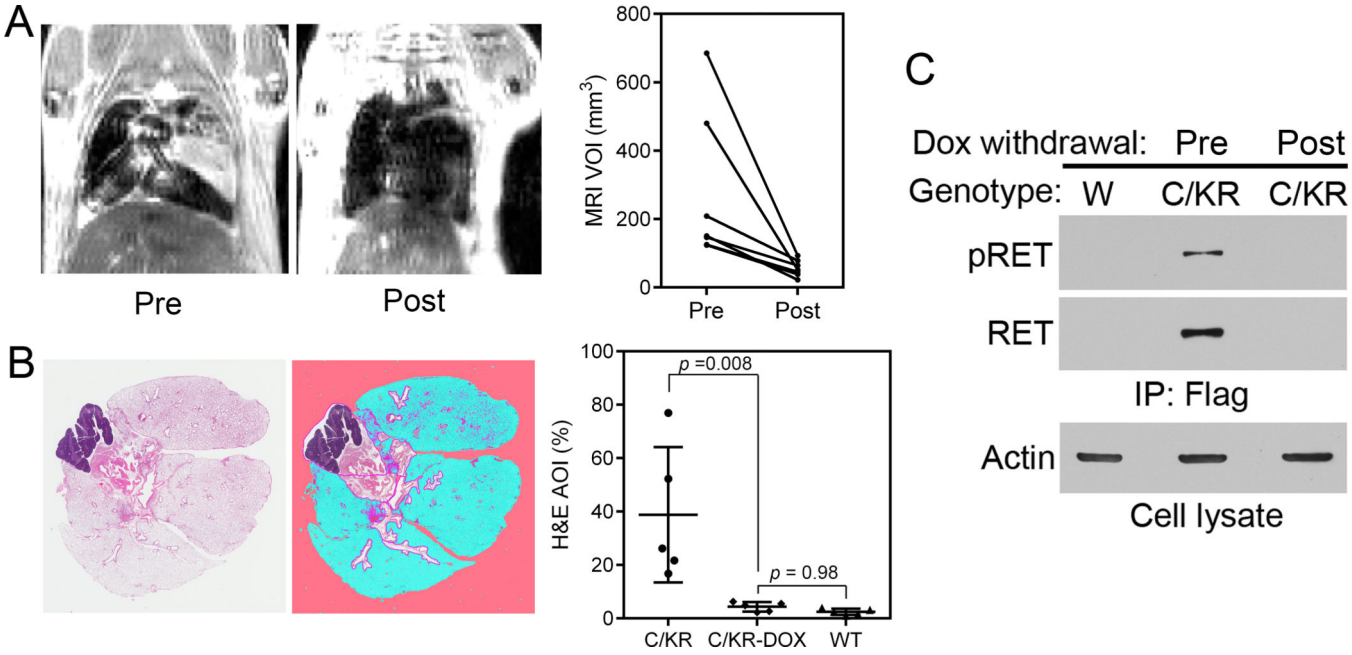

Figure 3.

KIF5B-RET expression is required to maintain lung tumors. A, C/KR mice developed MRI-detectable lung adenocarcinoma after Dox induction for 5 months. MRI images of representative tumor bearing mouse prior to and one month after Dox withdrawal. The graph shows comparison of MRI-detectable lung tumor burden prior to and post Dox withdrawal. Each line represents an individual mouse (n = 7). VOI, Volume of interest. B, H&E stained tissue section from lung of a mouse after Dox withdrawal (left). Lung tissue image from Genie® v1 histology pattern recognition software (Aperio) analysis (middle). Lung tumor burden was analyzed from H&E stained lung tissues (right) (n = 5 in each group). AOI, areas of interest. White, not lung tissue, area excluded; pink, background; blue, normal; purple: hyperplasia/neoplasia including some areas of normal bronchial epithelia (21). C, comparison of pRET and RET protein in the lungs of C/KR mice induced with Dox (prior to Dox withdrawal) and 1 month post Dox withdrawal. W, wildtype mouse.

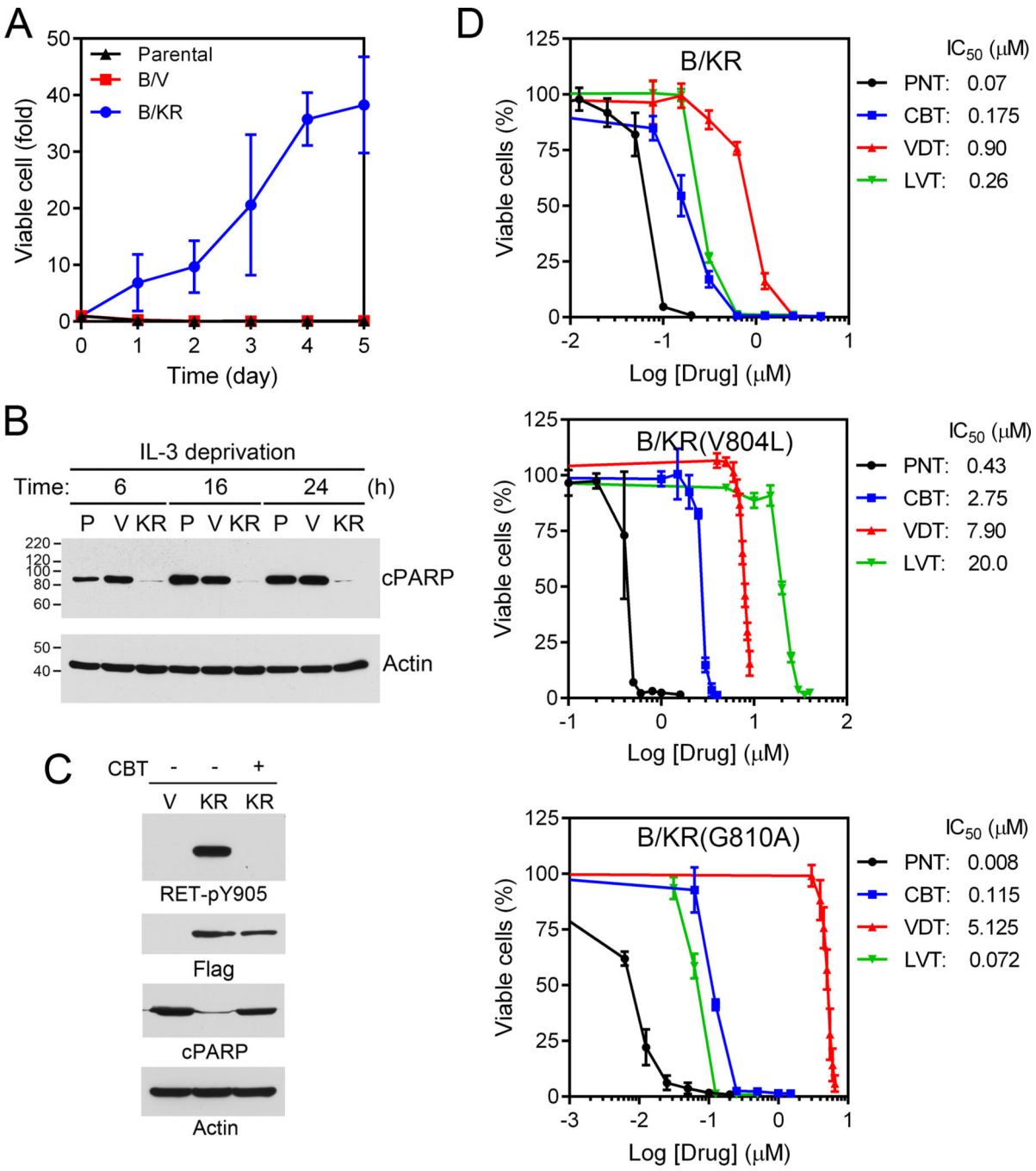

Figure 4.

Ponatinib is the most potent KIF5B-RET inhibitors and the vandetanib resistant RET^{G810A} mutation is hypersensitive to ponatinib. A, growth curve of parental, vector control (B/V) and stable BaF3 cells expressing KIF5B-RET (B/KR) without IL-3. B, cells were grown in medium without IL-3 for 6, 16, 24 hours. The cell lysates were immunoblotted with anti-cleaved PARP or anti-β actin. P, parental; V, vector control; KR, KIF5B-RET. C, vector control and KIF5B-RET cells were treated with or without 1 μM cabozantinib (CBT) for 3 hours. The cell lysates were immunoblotted with anti-RET-pY905, anti-Flag, anti-cleaved

PARP or anti-beta actin. D, Ba/F3 expressing KIF5B-RET, KIF5B-RET^{V804L}, or KIF5B-RET^{G810A} were seeded on 96-well plates and treated with indicated concentration of ponatinib (PNT), cabozantinib (CBT), vandetanib (VDT) or lenvatinib (LVT) for 5 days. Cell viability was measured using the CellTiter-Glo assay and IC_{50s} were determined. The data were from two triplicate experiments (n = 6).

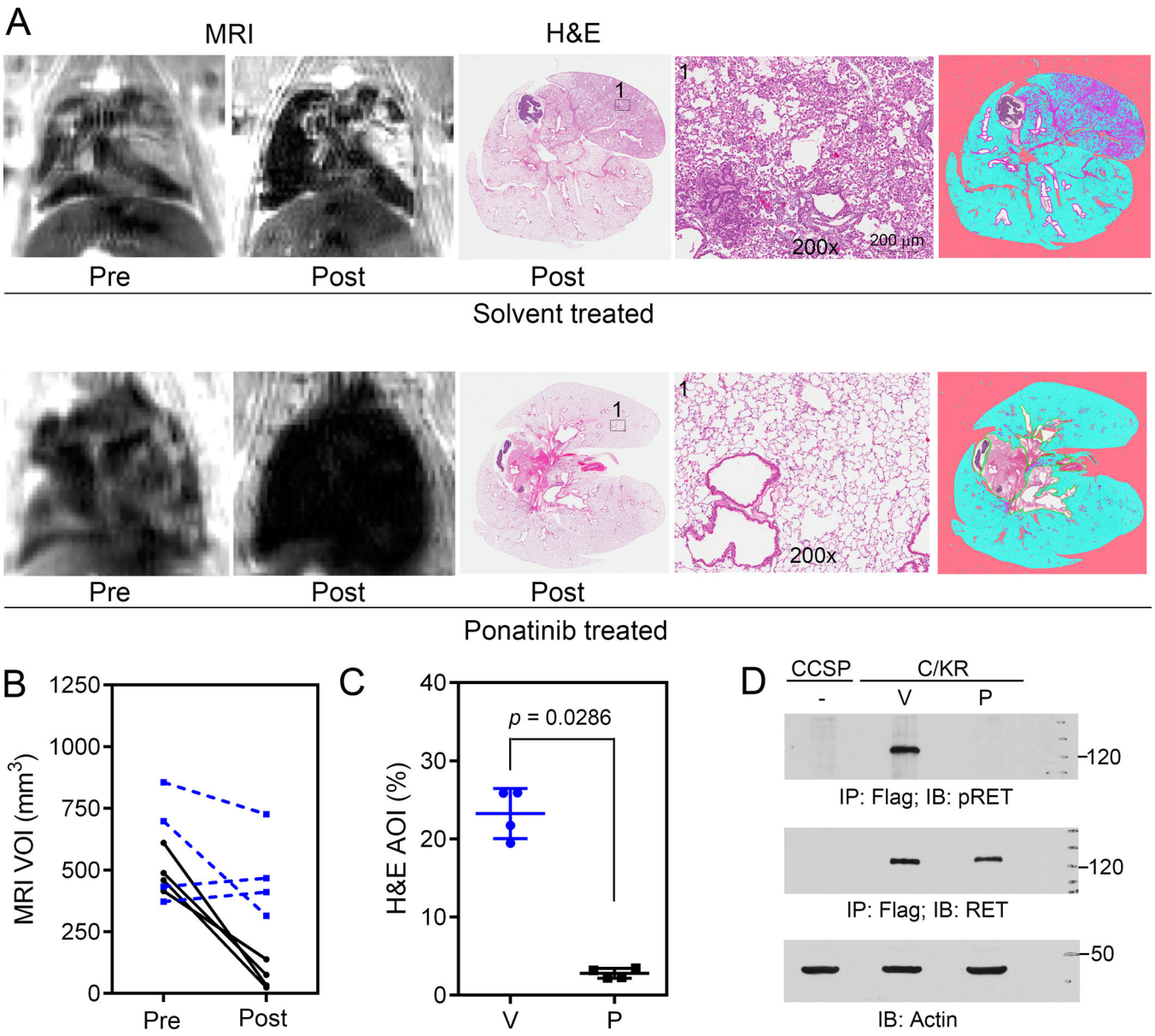

Figure 5.

Ponatinib treatment results in tumor regression. A, C/KR mice with MRI-detectable lung tumors were treated with vehicle (upper panel) or ponatinib (30 mg/kg/day, 5 days/week, p.o., lower panel) for 1 month and then analyzed by MRI again (n = 4 in each group). Lung tissue sections at the end point were stained with H&E. Representative images of MRI, H&E sections, and image from Genie® v1 histology pattern recognition software analysis (right) are shown. B, comparison of MRI-detectable lung tumor burden prior to and post vehicle or ponatinib treatment. Each line represents an individual mouse. Blue, vehicle-treated; Black, ponatinib-treated. C, lung tumor burden analyzed from samples of H&E stained lung tissue sections. V, vehicle-treated; P, ponatinib-treated. D, comparison of pRET, RET and β-actin

proteins in the lungs of CCSP and C/KR mice treated with vehicle or ponatinib. CCSP, negative control mouse.